Design of a Mid-IR Laser Based on a Ho:Nd-codoped Fluoroindate Fiber

Antonella Maria Loconsole, Mario Christian Falconi, Andrea Annunziato, Solenn Cozic, Samuel Poulain, and Francesco Prudenzano, *Member, IEEE*

***Abstract*—In this work, a novel mid-infrared continuous wave laser, based on a fluoroindate fiber co-doped with holmium and neodymium, is designed to emit at $\lambda_s = 3.92\ \mu$m, when pumped at $\lambda_p = 808$ nm. The laser is modeled considering a nine-level system, by taking into account experimental spectroscopical parameters. Since the energy transfer coefficients are unknown, they have been evaluated starting from the measured emission spectra of the bulk glass, reported in literature, and comparing their ratio with respect to the ratio between the simulated signal gain coefficients. The designed laser promises higher slope efficiency and power threshold lower than those obtainable with a holmium-heavily-doped fiber, having same fiber section geometry, same refractive indices and pumped at $\lambda_p = 888$ nm. Slope efficiency $\eta = 16.67\%$ and input power threshold $P_{th} = 0.2\ W$ are obtained for the fiber length $L_{fiber} = 0.4$ m, dopants concentrations $N_{Ho} = 8 \times 10^{26}$ ions/m^3 and $N_{Nd} = 1 \times 10^{26}$ ions/m^3, and output mirror reflectivity $R_{\text{out}} = 60\%$. This result encourages the fabrication of a continuous wave laser based on a Ho:Nd-codoped fluoroindate fiber.**

***Index Terms*—Electromagnetic design, fluoroindate glass, holmium, middle infrared (Mid-IR), neodymium, optical fiber lasers.**

I. Introduction

MID-INFRARED (MIR) emitting sources have attracted much interest during the last years, especially thanks to their multiple potential application such as fast communications, medical diagnostics and therapy, environmental monitoring, and sensing [1], [2], [3], [4], [5], [6], [7], [8], [9], [10]. These lasers can be designed and fabricated considering different fiber glasses, including chalcogenide and fluoride ones, doped or co-doped with different rare-earth ions, as thulium, holmium, dysprosium, erbium, neodymium, and praseodymium, for emission at different wavelengths [11], [12], [13], [14], [15], [16], [17], [18], [19], [20]. In particular, fluoroindate fibers exhibit high transparency in the $3-5\ \mu$m range, where many air pollutants and biomolecules exhibit light absorption peaks. The reduced optical attenuation $\alpha \approx 0.2$ dB/m from about $\lambda = 500$ nm to about $\lambda = 4500$ nm, and the low phonon energy of fluoroindate glasses make them good candidates for laser construction and exploitation [1], [15], [21]. In addition, they are good rare earth hosts, it is possible to incorporate also 10 mol.% of rare earth ions, similarly to fluorozirconate glasses. Erbium-, dysprosium-, and holmium-doped fluoroindate fibers have attracted particular attention for their emission at $\lambda = 3.5\ \mu$m, $\lambda = 4.2\ \mu$m, and $\lambda = 3.9\ \mu$m, respectively [13], [22], [23], [24], [25], [26], [27], [28]. Spectroscopical investigations on fluoroindate glasses co-doped with holmium-neodymium, holmium-europium, and praseodymium-ytterbium have shown that co-doping can lead to an improvement of the emission efficiency if compared to the employment of a single dopant. In particular, holmium-neodymium co-doping could allow better performance than those of heavily-holmium-doped, $N_{Ho} = 2 \times 10^{27}$ ions/m^3, fluoroindate fiber lasers [29], [30], [31], [32].

In this work, for the first time to the best of our knowledge, the design of a novel continuous wave (CW) laser, pumped at $\lambda_p = 808$ nm and emitting at $\lambda_s = 3.92\ \mu$m, based on a fluoroindate fiber co-doped with holmium and neodymium, is proposed. A model based on a nine-level system and taking into account the experimental spectroscopic parameters of the rare earth doped bulk glass, is developed [29], [33], [34], [35], [36], [37], [38]. The unknown energy transfer coefficients allowing to match the model with measured emission spectra are identified. The laser behavior is optimized by using a homemade numerical solver. The designed laser is very interesting, allowing simulated slope efficiency and input power threshold improved with respect to those obtained with a holmium-heavily-doped fiber, having the same fiber section geometry, same refractive indices, with a cavity length optimized at the pump wavelength $\lambda_p = 888$ nm.

II. Rate-Equation Model

The Ho:Nd-codoped fluoroindate fiber stimulated emission at $\lambda_s = 3.92\ \mu$m can be modeled by considering a nine-levels system, pumped at $\lambda_p = 808$ nm. The complete level scheme,

Manuscript received 20 July 2022; revised 13 September 2022 and 17 October 2022; accepted 24 October 2022. Date of publication 2 November 2022; date of current version 15 January 2023. This work was supported in part by MIUR PON R&I 2014-2020 "New Satellites Generation Components - NSG" under Cod. ID. ARS01_01215 NSG, in part by MIUR "Agriculture Green & Digital – AGREED," in part by PNR 2015–2020 under Grant ARS01_00254, and in part by H2020-ICT-37-2020 "Photonic Accurate and Portable Sensor Systems Exploiting Photo-Acoustic and Photo-Thermal Based Spectroscopy for Real-Time Outdoor Air Pollution Monitoring—PASSEPARTOUT" under Grant 101016956. *(Corresponding author: Francesco Prudenzano.)*

Antonella Maria Loconsole, Mario Christian Falconi, Andrea Annunziato, and Francesco Prudenzano are with the Department of Electrical and Information Engineering, Politecnico di Bari, 70125 Bari, Italy (e-mail: antonellamaria.loconsole@poliba.it; mariochristian.falconi@poliba.it; andrea.annunziato@poliba.it; francesco.prudenzano@poliba.it).

Solenn Cozic and Samuel Poulain are with the Le Verre Fluoré, 35170 Bruz, Brittany, France (e-mail: solenn.cozic@leverrefluore.eu; samuel.poulain@leverrefluore.eu).

Color versions of one or more figures in this article are available at https://doi.org/10.1109/JLT.2022.3218190.

Digital Object Identifier 10.1109/JLT.2022.3218190

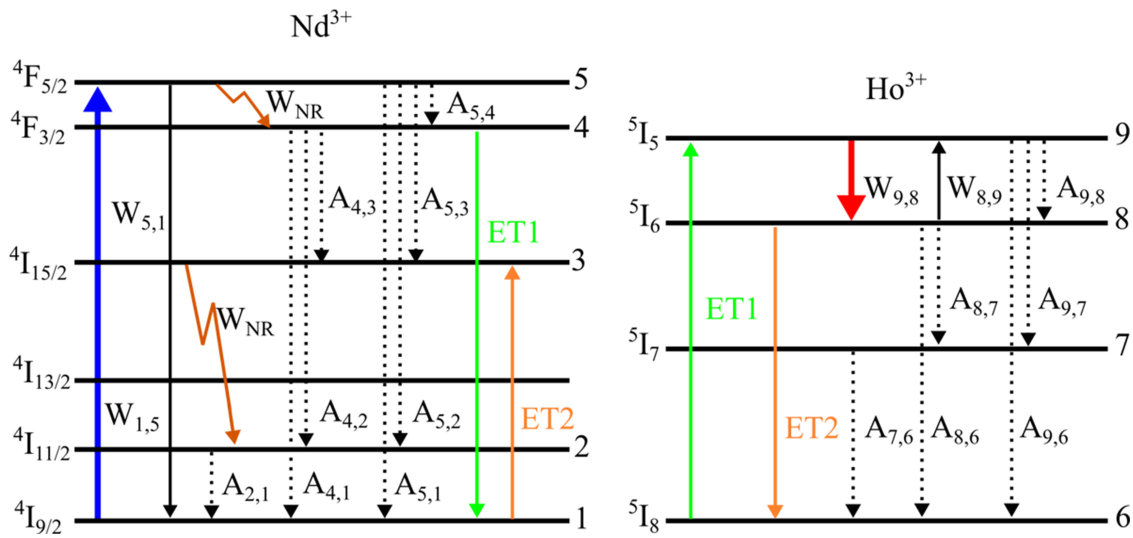

Fig. 1. Energy level scheme for the 9-level laser, pumped at $\lambda_p = 808$ nm, including pump absorption (transition 1-5, bold blue line) stimulated emission at $\lambda_s = 3920$ nm (transition 9-8, bold red line), radiative decays (dotted lines), nonradiative decays (transition 5-4 and transition 3-2, brown lines), and energy transfers (ET) (green and orange solid lines).

including all the significant ion interactions, is reported in Fig. 1. These are the pump absorption, the stimulated emission, the radiative and nonradiative decays, and the energy transfers (ET) between Ho^{3+} and Nd^{3+} ions [29].

By following the rate equations approach [12], [14], [24], the energy level populations $N_1, \ldots, N_5$ of neodymium can be written by the nonlinear system (1a)–(1j) below:

$$\frac{\partial N_1}{\partial t} = -W_{15}N_1 + W_{51}N_5 + A_{51}N_5 + A_{41}N_4 + A_{21}N_2 + K_{ET1}N_6N_4 - K_{ET2}N_8N_1 \quad (1a)$$

$$\frac{\partial N_2}{\partial t} = -\frac{1}{\tau_{R2}}N_2 + A_{52}N_5 + A_{42}N_4 + W_{NR}N_3 \quad (1b)$$

$$\frac{\partial N_3}{\partial t} = A_{53}N_5 + A_{43}N_4 + K_{ET2}N_8N_1 - W_{NR}N_3 \quad (1c)$$

$$\frac{\partial N_4}{\partial t} = -\frac{1}{\tau_{R4}}N_4 + A_{54}N_4 - K_{ET1}N_6N_4 + W_{NR}N_5 \quad (1d)$$

$$\frac{\partial N_5}{\partial t} = W_{15}N_1 - W_{51}N_5 - \frac{1}{\tau_{R5}}N_5 - W_{NR}N_5 \quad (1e)$$

whereas the energy level populations $N_6, \ldots, N_9$ of holmium can be written as

$$\frac{\partial N_6}{\partial t} = A_{96}N_9 + A_{86}N_8 + A_{76}N_7 - K_{ET1}N_6N_4 + K_{ET2}N_8N_1 \quad (1f)$$

$$\frac{\partial N_7}{\partial t} = -\frac{1}{\tau_{R7}}N_7 + A_{97}N_9 + A_{87}N_8 \quad (1g)$$

$$\frac{\partial N_8}{\partial t} = W_{98}N_9 - W_{89}N_8 - \frac{1}{\tau_{R8}}N_8 + A_{98}N_9 - K_{ET2}N_8N_1 \quad (1h)$$

$$\frac{\partial N_9}{\partial t} = -W_{98}N_9 + W_{89}N_9 - \frac{1}{\tau_{R9}}N_9 + K_{ET1}N_6N_4 \quad (1j)$$

where $A_{i,j} = \frac{\beta_{i,j}}{\tau_{Ri}}$ are the radiative decay rates; $\beta_{i,j}$ are the branching ratios; τ_{Ri} are the i-th level lifetimes; K_{ET1} and K_{ET2} are the ET coefficients; W_{NR} are the non-radiative decay rates. The emission/absorption transition rate $W_{i,j}$ for the $i \rightarrow j$ transition is defined as

$$W_{i,j}(z,t) = \frac{\sigma_{i,j}(\lambda_{p/s})}{\frac{hc_0}{\lambda_{p/s}}} \left[P^{\pm}_{p/s}(z,t)\right] \Gamma_{p/s} \quad (2)$$

where $\sigma_{i,j}(\lambda_{p/s})$ is the emission/absorption cross section at the wavelength $\lambda_{p/s}$ for the $i \rightarrow j$ (1-5, 5-1 and 8-9, 9-8) transitions; $\lambda_{p/s}$ is the pump/signal wavelength; h is the Plank constant; c_0 is the light speed in vacuum; $P^{\pm}_p$ is the forward/backward pump power; $P^{\pm}_s$ is the forward/backward signal power; Γ_p/Γ_s are the overlap coefficients between the pump/signal beam and the doped area A_d. The conditions $N_1 + N_2 + N_3 + N_4 + N_5 = N_{Nd}$ and $N_6 + N_7 + N_8 + N_9 = N_{Ho}$ are imposed, where N_{Ho} and N_{Nd} are the dopant concentrations.

The power propagation for pump and signal beams is governed by the following partial differential equations

$$\frac{\partial P_p}{\partial z} = [g_p(z) - \alpha]\; P_p(z) \quad (3a)$$

$$\frac{\partial P^{\pm}_s}{\partial z} = \pm [g_s(z) - \alpha]\; P^{\pm}_s(z) \quad (3b)$$

where

$$g_p(z) = [-\sigma_{15}(\nu_p) N_1(z) + \sigma_{51}(\nu_p) N_5(z)]\; \Gamma_p,$$

$$g_s(z) = [-\sigma_{89}(\nu_s) N_8(z) + \sigma_{98}(\nu_s) N_9(z)]\; \Gamma_s,$$

are the gain coefficients for the pump and the signal, respectively, and α is the glass optical background loss.

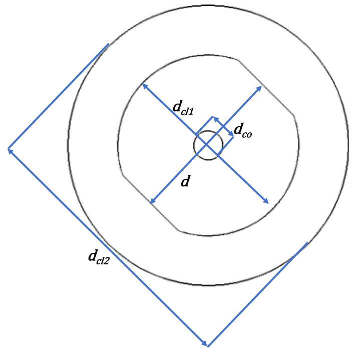

Fig. 2. Transverse section of the employed double cladding fiber.

To solve (3), the following boundary conditions are imposed.

$$P_p(0) = P_p^{\text{in}} \tag{4a}$$

$$P_s^+(0) = R_{\text{in}} P_s^-(0) \tag{4b}$$

$$P_s^-(L) = R_{\text{out}} P_s^+(L) \tag{4c}$$

where $z = 0$ and $z = L$ represent the ends of the laser cavity, P_p^{in} is the input pump power, R_{in} and R_{out} are the input and output mirror reflectivity, respectively. Initial conditions for level populations are also imposed as follows:

$$N_1(0) = N_{Nd} \tag{4d}$$

$$N_6(0) = N_{Ho} \tag{4e}$$

$$N_2(0) = N_3(0) = N_4(0) = N_5(0) = N_7(0) = N_8(0) = N_9(0) = 0 \tag{4f}$$

III. Energy Transfer Coefficients Recovering

The considered fiber is a step-index double-cladding fluoroindate (InF_3) glass fiber, doped with Ho^{3+} and Nd^{3+} ions. Its transverse section is shown in Fig. 2. The core diameter is $d_{co} = 16\ \mu\text{m}$. The cladding is 2-D shaped, obtained with circular diameter $d_{cl1} = 100\ \mu\text{m}$ truncated by two parallel planes at a distance $d = 90\ \mu\text{m}$, to enhance cladding pump absorption. The second cladding, made of low index resin, has diameter $d_{cl2} = 155\ \mu\text{m}$. The inner and outer numerical apertures are $NA_1 = 0.2$ and $NA_2 = 0.5$, respectively. The optical losses are conservatively considered $\alpha = 0.2\ \text{dB/m}$ for both pump and signal wavelengths, according to the measurement reported in [21]. This kind of double cladding fiber doped with holmium is produced by Le Verre Fluoré [21], [22]. In the following, the co-doping with Ho^{3+} and Nd^{3+} ions is supposed. The pump and signal wavelengths are $\lambda_p = 808\ \text{nm}$ and $\lambda_s = 3920\ \text{nm}$, respectively. The pump wavelength is feasible, since obtainable with commercial pigtailed semiconductor lasers.

The electromagnetic investigation, performed with a commercial Finite Element Method (FEM) solver, has shown that the fiber is slightly multimode at the normalized frequency number $V = 2.56$ of the signal wavelength. However, the second order mode can be neglected in the laser operation since its overlapping coefficient Γ_s is less than a half of the one of the fundamental mode; its contribution in the laser operation is not considered without significant error, as confirmed by preliminary simulation performed without any approximation [24].

TABLE I
Spectroscopic Parameters of Co-Doped Ho:Nd Fluoroindate Glass Fiber

Symbol	Value	Description
$\sigma_{15}(\lambda_p)$	$3.51 \times 10^{-24}\ m^2$ [33]	Absorption cross section $Nd: I_{9/2} \to F_{5/2}$
$\sigma_{51}(\lambda_p)$	$3.51 \times 10^{-24}\ m^2$ [33]	Emission cross section $Nd: F_{5/2} \to I_{9/2}$
$\sigma_{98}(\lambda_s)$	$3.4 \times 10^{-25}\ m^2$ [34]	Absorption cross section $Ho: I_6 \to I_5$
$\sigma_{89}(\lambda_s)$	$3.4 \times 10^{-25}\ m^2$ [34]	Emission cross section $Ho: I_5 \to I_6$
τ_{R2}	$\approx 0.01\ ms$ [35]	$Nd: I_{11/2}$ radiative lifetime
τ_{R4}	$0.943\ ms$ [33]	$Nd: F_{3/2}$ radiative lifetime
τ_{R5}	$0.315\ ms$ [33]	$Nd: F_{5/2}$ radiative lifetime
τ_{R7}	$9.09\ ms$ [36]	$Ho: I_7$ radiative lifetime
τ_{R8}	$3.66\ ms$ [29]	$Ho: I_6$ radiative lifetime
τ_{R9}	$0.29\ ms$ [29]	$Ho: I_5$ radiative lifetime
β_{21}	100% [33]	$Nd: I_{11/2} \to I_{9/2}$ branching ratio
β_{41}	63.7% [33]	$Nd: F_{3/2} \to I_{9/2}$ branching ratio
β_{42}	36.3% [33]	$Nd: F_{3/2} \to I_{11/2}$ branching ratio
β_{43}	$\approx$ 0% [33]	$Nd: F_{3/2} \to I_{15/2}$ branching ratio
β_{51}	62.6% [33]	$Nd: F_{5/2} \to I_{9/2}$ branching ratio
β_{52}	37.4% [33]	$Nd: F_{5/2} \to I_{11/2}$ branching ratio
β_{53}	$\approx$ 0% [33]	$Nd: F_{5/2} \to I_{15/2}$ branching ratio
β_{54}	$\approx$ 0% [33]	$Nd: F_{5/2} \to F_{3/2}$ branching ratio
β_{76}	100% [34]	$Ho: I_7 \to I_8$ branching ratio
β_{86}	94.0% [34]	$Ho: I_6 \to I_8$ branching ratio
β_{87}	6.00% [34]	$Ho: I_6 \to I_7$ branching ratio
β_{96}	55.7% [34]	$Ho: I_5 \to I_8$ branching ratio
β_{97}	43.0% [34]	$Ho: I_5 \to I_7$ branching ratio
β_{98}	1.30% [34]	$Ho: I_5 \to I_6$ branching ratio
W_{NR}	$\approx 10^8\ s^{-1}$ [37][38]	Non-radiative rates $Nd: F_{5/2} \to F_{3/2}$ and $Nd: F_{15/2} \to F_{11/2}$

The spectroscopic parameters used in the simulations are listed in Table I. They are taken from [29], [33], [34], [35], [36], [37], [38]. The ion rate equations and the power propagation equations are implemented in a home-made computer code to simulate the optical gain and the laser behavior. Since ET coefficients K_{ET1} and K_{ET2} are not available from literature, they have been evaluated starting from measured emission spectra from [29] of the bulk glass and comparing their ratio with respect to the gain coefficient ratio simulated for the fiber laser, as reported below. This approach was proposed in a previous work [39]. The aforesaid comparison is feasible in the linear region of the laser characteristic.

Fig. 3 shows the measured emission spectra intensities $s_{sn}(\lambda)$ for different Ho^{3+} concentrations [29], normalized with respect to $s_{s1}(\lambda)$ for a better reading; the Nd^{3+} concentration is set to $N_{Nd} = 2 \times 10^{26}\ \text{ions/m}^3$ (1 mol.%). In particular, $s_{s1}(\lambda)$ is the normalized emission spectrum intensity for $N_{Ho} = 2 \times 10^{26}\ \text{ions/m}^3$ (1 mol.%) (blue curve), $s_{s2}(\lambda)$ for $N_{Ho} = 1 \times 10^{26}\ \text{ions/m}^3$ (0.5 mol.%) (red curve), and $s_{s3}(\lambda)$ for $N_{Ho} = 4 \times 10^{25}\ \text{ions/m}^3$ (0.2 mol.%) (yellow curve). The ratios R_n between measured emission spectra at $\lambda_s = 3920\ \text{nm}$ are defined as in Table II. The signal gains coefficients $g_{s1}(\lambda_s)$, $g_{s2}(\lambda_s)$, and $g_{s3}(\lambda_s)$ refer to $N_{Ho} = 2 \times 10^{26}\ \text{ions/m}^3$ (1 mol.%), $N_{Ho} = 1 \times 10^{26}\ \text{ions/m}^3$ (0.5 mol.%), and $N_{Ho} = 4 \times 10^{25}\ \text{ions/m}^3$ (0.2 mol.%), respectively.

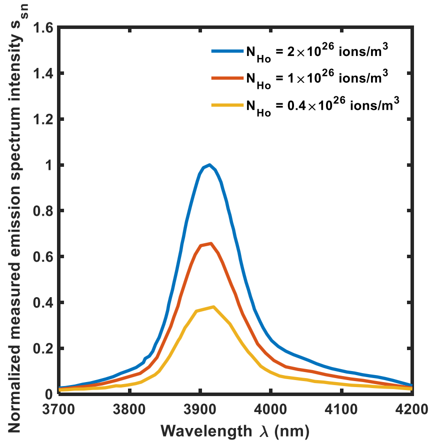

Fig. 3. Normalized measured emission spectra intensities s_{sn} as a function of the wavelength λ, for different Ho^{3+} concentrations; Nd^{3+} concentration is set to $N_{Nd} = 2 \times 10^{26}$ ions/m^3 (1 mol.%) [29].

TABLE II
EMISSION SPECTRA RATIOS

Symbol	Expression	Description
R_1	$s_{s1}(\lambda_s)/s_{s3}(\lambda_s)$	Ratio between the normalized emission spectra at signal wavelength for $N_{Ho} = 2 \times 10^{26}\ ions/m^3$ and $N_{Ho} = 4 \times 10^{25}\ ions/m^3$
R_2	$s_{s1}(\lambda_s)/s_{s2}(\lambda_s)$	Ratio between the normalized emission spectra at signal wavelength for $N_{Ho} = 2 \times 10^{26}\ ions/m^3$ and $N_{Ho} = 1 \times 10^{26}\ ions/m^3$
R_3	$s_{s2}(\lambda_s)/s_{s3}(\lambda_s)$	Ratio between the normalized emission spectra at signal wavelength for $N_{Ho} = 1 \times 10^{26}\ ions/m^3$ and $N_{Ho} = 4 \times 10^{25}\ ions/m^3$

TABLE III
EMISSION SPECTRA AND SIGNAL GAIN COEFFICIENT RATIOS COMPARISON

Emission spectra ratio R_n	Signal gain coefficient ratio RG_n
$R_1 = 2.63$	$RG_1 = 2.42$
$R_2 = 1.54$	$RG_2 = 1.51$
$R_3 = 1.62$	$RG_3 = 1.61$

The ratios RG_n are defined as follows $R\ G_1 = g_{s1}\ (\lambda_s)/g_{s3}(\lambda_s)$; $R\ G_2 = g_{s1}\ (\lambda_s)/g_{s2}(\lambda_s)$; $R\ G_3 = g_{s2}\ (\lambda_s)/g_{s3}(\lambda_s)$.

Fig. 4(a)–(c) show the colormaps of the percentage difference between the ratios $(R_n - RG_n)/R_n$ as a function of the trial energy transfer coefficients K_{ET1} and K_{ET2}. These three percentage differences must be contemporarily minimized. This condition is obtained for $K_{ET1} = 4 \times 10^{-22}$ m^3 ions^{-1} s^{-1} and $K_{ET2} = 6 \times 10^{-21}$ m^3 ions^{-1} s^{-1}, for which $(R_1 - RG_1)/R_1 = 8\%$, $(R_2 - RG_2)/R_2 = 1\%$, and $(R_3 - RG_3)/R_3 = 0.7\%$. Table III reports the simulated signal gain coefficient ratios RG_n for the recovered $K_{ET1} = 4 \times 10^{-22}$ m^3 ions^{-1} s^{-1} and $K_{ET2} = 6 \times 10^{-21}$ m^3 ions^{-1} s^{-1} compared to the measured emission spectra ratios R_n. The signal gain coefficient ratios RG_n are obtained considering the same average pump energy of [29], i.e., $P_p = 0.4\ W$, neodymium concentration $N_{Nd} = 2 \times 10^{26}$ ions/m^3 (1 mol.%), and holmium concentrations $N_{Ho} = 2 \times 10^{26}$ ions/m^3 (1 mol.%), $N_{Ho} = 1 \times 10^{26}$ ions/m^3 (0.5 mol.%), and $N_{Ho} = 0.4 \times 10^{26}$ ions/m^3 (0.2 mol.%). This allows a proper comparison with R_n.

To validate these results, the global $Ho : I_5$ level lifetime τ'_{R9} and the global $Ho : I_6$ level lifetime τ'_{R8} have been simulated and compared with the experimental ones taken from literature [29], for different holmium concentrations N_{Ho}. The lifetimes have been simulated solving the rate equations (1a)-(1j) as a function of time, pumping the system until the ion populations steady-state condition. Then, the pump power is turned off, setting $P_p = 0\ W$, and the simulated population exponential decays are observed. The level lifetimes are calculated as the time constants of the obtained exponential curves.

Fig. 5 shows the $Ho : I_5$ level lifetime τ'_{R9} and the $Ho : I_6$ level lifetime τ'_{R8} simulated (blue) and measured (red) [29] as a function of the holmium concentration N_{Ho}. The good accordance confirms that the recovered energy transfer coefficients K_{ET1} and K_{ET2} are correct.

IV. LASER DESIGN

In the design, a deep investigation of the laser output signal power P_s versus: i) the laser fiber length L_{fiber}; ii) the dopants concentration N_{Nd} and N_{Ho}; iii) the output mirror reflectivity R_2 is carried out, in order to identify the configuration allowing the maximum slope efficiency η and the minimum threshold power P_{th}.

Fig. 6 shows the output power P_s as a function of the input pump power P_p, for different values of the fiber length L_{fiber}. The characteristics show a discontinuity with a sawtooth shape in all cases. The reason behind this behavior will be deeply investigated in Section V. The discontinuity shifts towards higher pump power as the fiber length L_{fiber} increases. Moreover, the slope efficiency η slightly decreases, while the input pump threshold is close to $P_{th} = 0.5\ W$ in all cases. It is worthy to observe that experiments in literature suggest avoiding input power larger than $P_p = 6\ W$ in typical fluoroindate fibers [22]. In a lightly doped fiber higher pumping levels could be potentially employed. Therefore, a different cavity optimization could be required. A good trade-off length is $L_{fiber} = 0.4$ m, for which the discontinuity occurs beyond the realistic range of power, i.e., for $P_p = 8\ W$, and for which the efficiency $\eta = 8.47\%$ is obtained. The slope efficiency is calculated after the threshold, between $P_p = 1\ W$ and $P_p = 1.5\ W$.

Fig. 7 shows the output power P_s as a function of the input pump power P_p, for different values of the holmium concentration N_{Ho}. As the concentration increases, the slope efficiency η also increases and the discontinuity shifts to higher input pump powers. The input pump threshold decreases to $P_{th} = 0.1\ W$. The optimal holmium concentration is the maximum considered in the simulations $N_{Ho} = 8 \times 10^{26}$ ions/m^3 (4 mol.%) (purple curve). Generally, higher holmium concentrations are not used in practice to avoid second order phenomena, such as cross-relaxation or up-conversion.

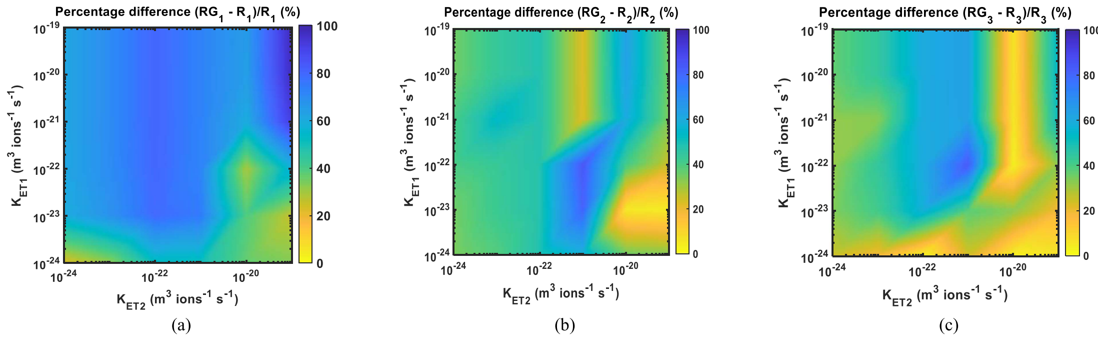

Fig. 4. (a) Percentage difference $(RG_1 - R_1)/R_1$, (b) percentage difference $(RG_2 - R_2)/R_2$, and (c) percentage difference $(RG_3 - R_3)/R_3$ as a function of energy transfer coefficients K_{ET1} and K_{ET2}.

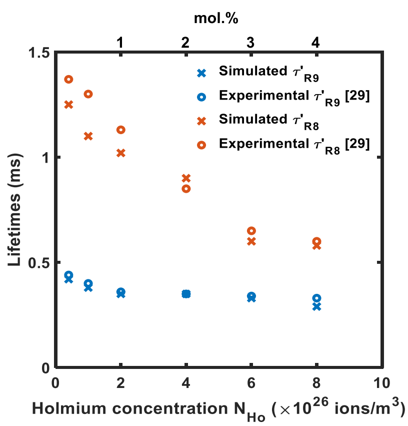

Fig. 5. $Ho : I_5$ level lifetime τ'_{R9} and the $Ho : I_6$ level lifetime τ'_{R8} as a function of the holmium concentration N_{Ho}, comparing simulated (blue) and measured [29] (red) values; $N_{Nd} = 2 \times 10^{26}$ ions/m^3 (1 mol.%).

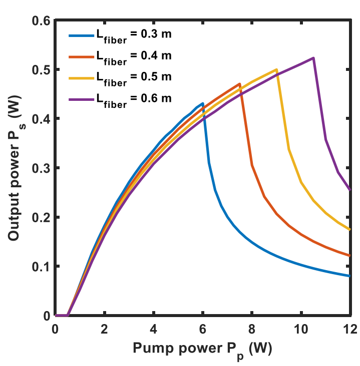

Fig. 6. Output power P_s as a function of the input pump power P_p, for different values of the fiber length L_{fiber}. Holmium concentration $N_{Ho} = 2 \times 10^{26}$ ions/m^3 (1 mol.%), neodymium concentration $N_{Nd} = 2 \times 10^{26}$ ions/m^3 (1 mol.%), input mirror reflectivity $R_{\mathrm{in}} = 99\%$, output mirror reflectivity $R_{\mathrm{out}} = 70\%$.

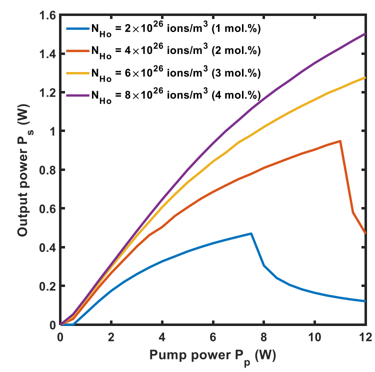

Fig. 7. Output power P_s as a function of the input pump power P_p, for different values of the holmium concentration N_{Ho}. Fiber length $L_{fiber} = 0.4$ m, neodymium concentration $N_{Nd} = 2 \times 10^{26}$ ions/m^3 (1 mol.%), input mirror reflectivity $R_{\mathrm{in}} = 99\%$, output mirror reflectivity $R_{\mathrm{out}} = 70\%$.

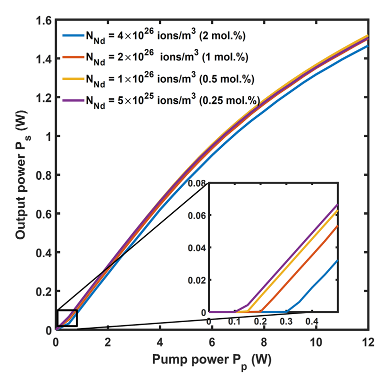

Fig. 8. Output power P_s as a function of the input pump power P_p, for different values of the neodymium concentration N_{Nd}. Fiber length $L_{fiber} = 0.4$ m, holmium concentration $N_{Ho} = 8 \times 10^{26}$ ions/m^3 (4 mol.%), input mirror reflectivity $R_{\mathrm{in}} = 99\%$, output mirror reflectivity $R_{\mathrm{out}} = 70\%$.

Fig. 8 shows the output power P_s as a function of the input pump power P_p, for different values of neodymium concentration N_{Nd}. As the concentration increases, the slope efficiency η slightly increases until $N_{Nd} = 1 \times 10^{26}$ ions/m^3 (0.5 mol.%) (yellow curve), while the input pump threshold P_{th} always decreases. The value $N_{Nd} = 1 \times 10^{26}$ ions/m^3 (0.5 mol.%) can be considered as optimized, allowing the highest efficiency and a good input pump threshold $P_{th} = 0.15\ W$.

Fig. 9 shows the output power P_s as a function of the input pump power P_p, for different values of output mirror reflectivity R_{out}. The slope efficiency η increases as the output mirror reflectivity R_{out} decreases until $R_{\mathrm{out}} = 60\%$, while the input pump threshold P_{th} decreases from $P_{th} = 0.3\ W$ to $P_{th} = 0.05\ W$.

The optimal laser configuration is obtained for fiber length $L_{fiber} = 0.4$ m, holmium concentration $N_{Ho} = 8 \times 10^{26}$ ions/m^3, neodymium concentration $N_{Nd} = 1 \times 10^{26}$ ions/m^3, and output mirror reflectivity $R_{\mathrm{out}} = 60\%$,

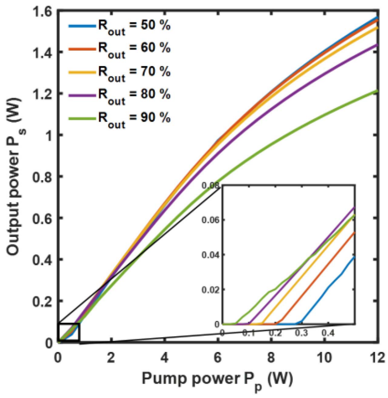

Fig. 9. Output power P_s as a function of the input pump power P_p, for different values of the output mirror reflectivity R_{out}. Fiber length $L_{fiber} = 0.4$ m, holmium concentration $N_{Ho} = 8 \times 10^{26}$ ions/m^3 (4 mol.%), neodymium concentration $N_{Nd} = 1 \times 10^{26}$ ions/m^3 (0.5 mol.%), input mirror reflectivity $R_{\text{in}} = 99\%$.

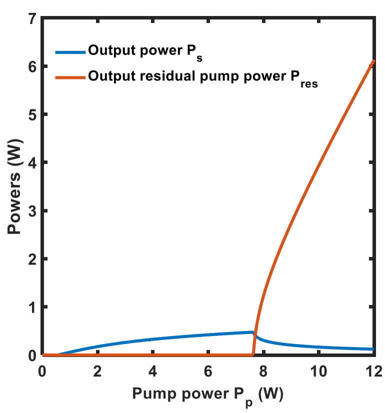

Fig. 10. Output power P_s (blue curve) and output residual pump power P_{res} (red curve) as a function of the input pump power P_p. Fiber length $L_{fiber} = 0.4$ m, holmium concentration $N_{Ho} = 2 \times 10^{26}$ ions/m^3 (1 mol.%), neodymium concentration $N_{Nd} = 2 \times 10^{26}$ ions/m^3 (1 mol.%), input mirror reflectivity $R_{\text{in}} = 99$ %, output mirror reflectivity $R_{\text{out}} = 70$ %.

allowing the slope efficiency $\eta = 16.67\%$ and the input pump threshold $P_{th} = 0.2\ W$. These simulated performances are better than those typical of CW lasers obtained with heavily-holmium-doped fiber with the same geometry, pumped at $\lambda_p = 888$ nm, showing $\eta = 10.2\%$ and input pump threshold $P_{th} = 4.3\ W$ [22].

V. Results Discussion

By the inspection of the energy level diagram of Fig. 1, for each ion couple involved in the ET2 transition an energy loss equal to the energy difference $\Delta E = 1.7 \times 10^3$ cm^{-1} [29] between level 8 and level 3 occurs, due to the 1-3 and 8-6 transitions. This energy leakage could be the cause of the sawtooth. Indeed, simulating the system without ET2 effect, by putting null K_{ET2}, the laser shows the typical characteristic with a pump threshold $P_{th} = 0.6\ W$, a slope efficiency $\eta = 0.2\%$, and a saturation power $P_{ss} = 4.3\ W$, without any sawtooth.

Fig. 10 shows the output power P_s (blue curve) and the output residual pump power P_{res} at the end of the fiber (red curve) as a function of the input pump power P_p. The output residual pump power P_{res} steeply increases when the output signal P_s shows the discontinuity, close to $P_p = 7.5\ W$. For larger values of the input pump power P_p, a large amount is not absorbed, reaching about the 50% for $P_p = 12\ W$. This is plausibly caused by a too large depopulation of level 1 ($Nd:\ I_{9/2}$), reducing ET2 effect. By simulation, the N_1 ion population at the end of the fiber steeply decreases for pump power higher than $P_p = 7.5\,W$. Therefore, few ions can be promoted from level 1 to level 3 ($Nd:\ I_{15/2}$) and the related transition 8-6 does not occur efficiently. Accordingly with this phenomenon, for pump power larger than $P_p = 7.5\ W$, the N_8 ion population steeply increases affecting the laser population inversion. This could be a further cause of the sawtooth.

VI. Conclusion

For the first time, a CW laser emitting at $\lambda_s = 3.92\ \mu$m based on a holmium and neodymium co-doped fluoroindate glass fiber is accurately designed, by using measured and recovered spectroscopic parameters. By employing an input pump power at the wavelength $\lambda_p = 808$ nm, a fiber length $L_{fiber} = 0.4$ m, an holmium concentration $N_{Ho} = 8 \times 10^{26}$ ions/m^3 (4 mol.%), a neodymium concentration $N_{Nd} = 1 \times 10^{26}$ ions/m^3 (0.5 mol.%), and an output mirror reflectivity $R_{\text{out}} = 60\%$, a slope efficiency $\eta = 16.67\%$ and an input pump threshold $P_{th} = 0.2\ W$ can be obtained. This result is interesting if compared with the efficiency obtainable with holmium doped fiber.

References

[1] L. Zhang, F. Guan, L. Zhang, and Y. Jiang, "Next generation mid-infrared fiber: Fluoroindate glass fiber," *Opt. Mater. Exp.*, vol. 12, no. 4, pp. 1683–1707, Mar. 2022.

[2] Q. Luo et al., "Remote sensing of pollutants using femtosecond laser pulse fluorescence spectroscopy," *Appl. Phys. B*, vol. 82, pp. 105–109, Nov. 2005.

[3] S. B. Mirov et al., "Frontiers of Mid-IR lasers based on transition metal doped chalcogenides," *IEEE J. Sel. Topics Quantum Electron.*, vol. 24, no. 5, pp. 1–29, Sep./Oct. 2018.

[4] A. E. Klingbeil, J. B. Jeffries, and R. K. Hanson, "Temperature-dependent mid-IR absorption spectra of gaseous hydrocarbons," *J. Quant. Spectrosc. Radiat. Transf.*, vol. 107, pp. 407–420, Oct. 2007.

[5] J. M. Bakker et al., "The mid-IR absorption spectrum of gas-phase clusters of the nucleobases guanine and cytosine," *Phys. Chem. Chem. Phys.*, vol. 6, no. 10, pp. 2810–2815, Apr. 2004.

[6] K. Wang, D.-W. Sun, and H. Pu, "Emerging non-destructive terahertz spectroscopic imaging technique: Principle and applications in the agri-food industry," *Trends Food Sci. Technol.*, vol. 67, pp. 93–105, Sep. 2017.

[7] Z. Zhou et al., "Towards high-power mid-IR light source tunable from 3.8 to 4.5 μm by HBr-filled hollow-core silica fibres," *Light: Sci. Appl*, vol. 11, Jan. 2022, Art. no. 15.

[8] R. M. Schwartz, D. Woodbury, J. Isaac, P. Sprangle, and H. M. Milchberg, "Remote detection of radioactive material using mid-IR laser–driven electron avalanche," *Sci. Adv.*, vol. 5, no. 3, Mar. 2019, Art. no. eaav6804.

[9] M. C. Falconi, D. Laneve, M. Bozzetti, T. T. Fernandez, G. Galzerano, and F. Prudenzano, "Design of an efficient pulsed dy^{3+}: ZBLAN fiber laser operating in gain switching regime," *J. Lightw. Technol.*, vol. 36, no. 23, pp. 5327–5333, Sep. 2018.

[10] L. Sójka et al., "High peak power Q-switched Er:ZBLAN fiber laser," *J. Lightw. Technol.*, vol. 39, no. 20, pp. 6572–6578, Jul. 2021.

[11] E. A. Anashkina, "Laser sources based on rare-earth ion doped tellurite glass fibers and microspheres," *Fibers*, vol. 8, no. 30, pp. 1–17, May 2020.

[12] M. C. Falconi et al., "Dysprosium-doped chalcogenide master oscillator power amplifier (MOPA) for mid-IR emission," *J. Lightw. Technol.*, vol. 35, no. 2, pp. 265–273, Jan. 2017.

[13] M. R. Majewski, R. I. Woodward, J.-Y. Carrée, S. Poulain, M. Poulain, and S. D. Jackson, "Emission beyond 4 μm and mid-infrared lasing in a dysprosium-doped indium fluoride (InF_3) fiber," *Opt. Lett.*, vol. 43, no. 8, pp. 1926–1929, 2018.

[14] Y. Wang et al., "Ultrafast dy^{3+}:Fluoride fiber laser beyond 3 μm," *Opt. Lett.*, vol. 44, pp. 395–398, Jan. 2019.

[15] M. Saad, R. Pafchek, P. Foy, Z. Jiang, D. Gardner, and P. Hawkins, "Indium fluoride glass fibers for mid-infrared applications," in *Proc. WSOF2015*, 2015, Art. no. WW4A.3.

[16] J. Pisarska, "IR transmission and emission spectra of erbium ions in fluoroindate glass," *J. Non-Cryst. Solids*, vol. 345-346, pp. 382–385, Oct. 2004.

[17] V. A. Jerez, C. B. de Araujo, and Y. Messaddeq, "Dynamics of energy transfer and frequency upconversion in Tm^{3+} doped fluoroindate glass," *J. Appl. Phys.*, vol. 96, no. 5, pp. 2530–2534, Sep. 2004.

[18] L. J. Borrero-Gonzalez, G. Galleani, D. Manzani, L. A. O. Nunes, and S. J. L. Ribeiro, "Visible to infrared energy conversion in Pr^{3+}-Yb^{3+} co-doped fluoroindate glasses," *Opt. Mater.*, vol. 35, no. 12, pp. 2085–2089, Oct. 2013.

[19] M. Kochanowicz et al., "Near-IR and mid-IR luminescence end energy transfer in fluoroindate glasses co-doped with Er^{3+}/Tm^{3+}," *Opt. Mater. Exp.*, vol. 9, no. 12, pp. 4772–4781, Dec. 2019.

[20] M. Kochanowicz et al., "Sensitization of Ho^{3+}-doped fluoroindate glasses for near and mid-infrared emission," *Opt. Mater.*, vol. 101, Mar. 2020, Art. no. 109707.

[21] Le Verre Fluoré, Catalog, Bruz, Brittany, France, 2019. [Online]. Available: https://leverrefluore.com/wp-content/uploads/2019/06/CatalogLVF-2019.pdf

[22] F. Maes et al., "Room-temperature fiber laser at 3.92 μm," *Optica*, vol. 5, no. 7, pp. 761–764, Jul. 2018.

[23] F. Zhou, J. Li, H. Luo, F. Quellette, and Y. Liu, "Numerical analysis of 3.92 μm dual-wavelength pumped heavily-holmium-doped fluoroindate fiber lasers," *J. Lightw. Technol*, vol. 39, no. 2, pp. 633–645, Jan. 2021.

[24] A. M. Loconsole, M. C. Falconi, V. Portosi, and F. Prudenzano, "Numerical design of a gain-switched pulsed laser at 3.92 μm wavelength based on a Ho3+-Doped fluoroindate fiber," *J. Lightw. Technol.*, vol. 39, no. 10, pp. 3276–3283, May 2021.

[25] M. R. Majewski and S. D. Jackson, "Numerical design of 4 μm-Class dysprosium fluoride fiber lasers," *J. Lightw. Technol.,* vol. 39, no. 15, pp. 5103–5110, May 2021.

[26] P. Wang et al., "3.5 μm emission in Er3+ doped fluoroindate glasses under 635 nm laser excitation," *J. Lumin.*, vol. 237, Sep. 2021, Art. no. 118200.

[27] H. He, Z. Jia, T. Wang, Y. Ohishi, W. Qin, and G. Qin, "Intense emission at $\sim$3.3 μm from Er3+-doped fluoroindate glass fiber," *Opt. Lett.*, vol. 46, no. 5, pp. 1057–1060, Feb. 2021.

[28] M. C. Falconi, A. M. Loconsole, A. Annunziato, S. Cozic, S. Poulain, and F. Prudenzano, "Design of an Er^{3+}:InF_3 fiber laser pumped with red light," *Proc. SPIE*, Strasbourg, France, vol. 12142, Apr. 2022, Art. no. 121420Z.

[29] R. Wang et al., "3.9 μm emission and energy transfer in ultra-low OH^-, Ho^{3+}/Nd^{3+} co-doped fluoroindate glasses," *J. Lumin.*, vol. 225, Sep. 2020, Art. no. 117363.

[30] Z. Zhang et al., "Enhanced 3.9 μm emission from diode pumped Ho^{3+}/Eu^{3+} codoped fluoroindate glasses," *Opt. Lett.*, vol. 46, no. 9, pp. 2031–2034, Apr. 2021.

[31] H. He, Z. Jia, Y. Ohishi, W. Qin, and G. Qin, "Efficient $\sim$4 μm emission from Pr3+/Yb3+ co-doped fluoroindate glass," *Opt. Lett.*, vol. 46, no. 22, pp. 5607–5610, Nov. 2021.

[32] A. M. Loconsole, M. C. Falconi, A. Annunziato, S. Cozic, S. Poulin, and F. Prudenzano, "Feasibility investigation of Ho:Nd codoped InF_3 fibers pumped at 808 nm wavelength," *Proc. SPIE*, Strasbourg, France, vol. 12142, Apr. 2022, Art. no. 1214210.

[33] A. Florez, J. F. Martinez, M. Florez, and P. Porcher, "Optical transition propabilities and compositional dependence of Judd-Ofelt parameters of Nd3+ ions in fluoroindate glasses," *J. Non-Cryst. Solids*, vol. 284, pp. 261–267, 2001.

[34] L. Gomes et al., "The basic spectroscopic parameters of ho^{3+}-doped fluoroindate glass for emission at 3.9 μm," *Opt. Mater.*, vol. 60, pp. 618–626, Sep. 2016.

[35] Y. V. Orlovskii, T. T. Basiev, and K. K. Pukhov, "Multiphonon relaxation in fluoride and ternary sulfide laser crystals with neodymium ions," *J. Exp. Theor. Phys.*, vol. 106, 2008, Art. no. 661.

[36] A. Florez, S. L. Oliveira, M. Florez, L. A. Gomez, and L. A. O. Nunes, "Spectroscopic characterization of Ho^{3+} ion-doped fluoride glass," *J. Alloys Compd.*, vol. 418, pp. 238–242, Feb. 2006.

[37] Y. V. Orlovskii, R. J. Reeves, R. C. Powell, T. T. Basiev, and K. K. Pukhov, "Multiple-phonon non-radiative relaxation: Experimental rates in fluoride crystals doped with Er3+ and Nd3+ ions and theoretical model," *Phys. Rev. B*, vol. 49, no. 6, Feb. 1994, Art. no. 3821.

[38] L. de S. Menezes, G. S. Maciel, C. B. de Araújo, and Y. Messaddeq, "Thermally enhanced frequency upconversion in Nd3+-doped fluoroindate glass," *J. Appl. Phys.*, vol. 90, no. 9, pp. 4498–4501, 2001.

[39] M. C. Falconi et al., "Design of active devices based on rare-earth-doped glass/glass ceramic: From the material characterization to the device parameter refinement," *Proc. SPIE*, France, vol. 11357, Apr. 2020, pp. 39–45.

Antonella Maria Loconsole received the M.Sc. degree in telecommunications engineering (*cum laude*) in 2019 from the Politecnico di Bari, Bari, Italy, where she is currently working toward the Ph.D. degree in electrical and information engineering. Her research interests include SIW antennas, microwave applicators for medical applications, and optical fiber lasers and amplifiers.

Mario Christian Falconi received the M.Sc. degree in electronic engineering (*cum laude*) and the Ph.D. degree in electrical and information engineering from the Politecnico di Bari, Bari, Italy, in 2015 and 2019, respectively. In 2019, he was a Research Fellow and is currently a Research Assistant of electromagnetic fields with the Department of Electrical and Information Engineering, Politecnico di Bari. His research interests include fiber lasers and amplifiers, photonic crystal fibers, and nonlinear effects in optical fibers.

Andrea Annunziato received the M.Sc. degree in electronic engineering (*cum laude*) in 2020 from the Politecnico di Bari, Bari, Italy, where he is currently working toward the Ph.D. degree in aerospace sciences and engineering. His research interests include optical fiber sensors, lasers, and amplifiers.

Solenn Cozic received the Ph.D. degree in material science from Rennes 1 University, Rennes, France, in 2016. She is currently a Research and Development Engineer with Le Verre Fluoré. Her research interests include development of novel fluoride glasses, optical fibers and fluoride glass fiber components for mid infrared, and visible fiber lasers applications.

Samuel Poulain received the Engineering Master degree from ENSTA ParisTech, Palaiseau, France, in 1997. After 15 years with Automotive Industry as an Engineer, he became the General Manager of Le Verre Fluoré in 2015. He is involved in various scientific developments, in particular in mid-IR supercontinuum generation and mid-IR fiber lasers.

Francesco Prudenzano (Member ,IEEE) received the Ph.D. degree in electronic engineering from the Politecnico di Bari, Bari, Italy, in November 1996. Since 2018, he has been a Full Professor of electromagnetic fields with the Department of Electrical and Information Engineering, Politecnico di Bari. His research interests include regards the design and characterization of microwave devices, integrated optics, and optical fiber-based devices. He is the Head of Microwave and Optical Engineering Group, Department of Electrical and Information Engineering, Politecnico di Bari. From 2017 to 2018, he was the Chair of SIOF, Italian Society of Optics and Photonics (Italian branch of EOS - European Optical Society). He has coauthored more than 400 publications, 295 of which got published in journals and international conferences, lectures, and invited papers. He is involved in several national and international research projects and cooperations.

Open Access provided by 'Politecnico di Bari' within the CRUI CARE Agreement